meteorology

MDPI

Article

Anomaly-Based Variable Models: Examples of Unusual Track and Extreme Precipitation of Tropical Cyclones

Weihong Qian [1,*], Jun Du [2], Yang Ai [1], Jeremy Leung [1], Yongzhu Liu [3] and Jianjun Xu [4,5,*]

[1] Department of Atmospheric and Oceanic Sciences, Peking University, Beijing 100871, China; aiyang@pku.edu.cn (Y.A.); chleung@pku.edu.cn (J.L.)
[2] Environmental Modeling Center, National Centers for Environmental Predictions, National Oceanic and Atmospheric Administration, College Park, MD 20740, USA; jun.du@noaa.gov
[3] Earth System Modeling and Prediction Centre, China Meteorological Administration, Beijing 100081, China; liuyzh@cma.gov.cn
[4] Shenzhen Institute of Guangdong Ocean University, Shenzhen 518120, China
[5] South China Sea Institute of Marine Meteorology, Guangdong Ocean University, Zhanjiang 524088, China
* Correspondence: qianwh@pku.edu.cn (W.Q.); jxu@gdou.edu.cn (J.X.)

Abstract: Tropical cyclones (TCs) can cause severe wind and rain hazards. Unusual TC tracks and their extreme precipitation forecasts have become two difficult problems faced by conventional models of primitive equations. The case study in this paper finds that the numerical computation of the climatological component in conventional models restricts the prediction of unusual TC tracks. The climatological component should be a forcing quantity, not a predictor in the numerical integration of all models. Anomaly-based variable models can overcome the bottleneck of forecast time length or the one-week forecasting barrier, which is limited to less than one week for conventional models. The challenge in extreme precipitation forecasting is how to physically get the vertical velocity. The anomalous moisture stress modulus (AMSM), as an indicator of heavy rainfall presented in this paper, considers the two conditions associated with vertical velocity and anomalous specific humidity in the lower troposphere. Vertical velocity is produced by the orthogonal collision of horizontal anomalous airflows.

Keywords: tropical cyclone; anomalous track; extreme precipitation; anomaly-based variable; orthogonal collision; one-week forecasting barrier

Citation: Qian, W.; Du, J.; Ai, Y.; Leung, J.; Liu, Y.; Xu, J. Anomaly-Based Variable Models: Examples of Unusual Track and Extreme Precipitation of Tropical Cyclones. *Meteorology* **2024**, *3*, 243–261. https://doi.org/10.3390/meteorology3020013

Academic Editor: Paul D. Williams

Received: 21 April 2024
Revised: 31 May 2024
Accepted: 5 June 2024
Published: 17 June 2024

1. Introduction

Every summer and autumn, several typhoons and hurricanes, respectively, make landfall in China and the US, bringing strong winds and heavy rainfall (Maxwell et al., 2021 [1]; Li and Zhao, 2022 [2]). Therefore, the forecasting of wind and rainfall associated with tropical cyclones (TCs) has become a key task of meteorological agencies. It is well-known that the accuracy of TC-related wind and rain forecasts depends on the accuracy of TC track prediction (Marchok, 2021 [3]; Conroy et al., 2023 [4]). For normal TC tracks, forecasters can predict them several days in advance. However, for a small number of unusual TCs, their track forecast becomes a problem even with lead times of 1–2 days (Qian C. H. et al., 2013 [5]; Yu et al., 2021 [6]). In addition, whether a TC moves along a usual or unusual trajectory and accurate areal distribution of precipitation are challenges in the current numerical weather prediction (NWP) models.

An example of extreme TC-induced precipitation is caused by the Super Typhoon Megi in 2010 that had an unusual track (Qian C. H. et al., 2013 [5]). Megi (2010) moved west–northwestwards from 13 to 16 October 2010. On 16 to 17 October, it experienced a slow left turning and moved in a southwest–west direction. On 18 to 19 October, it reached the maximum intensity before landing in the northern Philippines and resulted in extensive damage to both human lives and property. During 19 and 20 October, it rapidly turned right

with an angle greater than 90 degrees in the South China Sea (SCS). Then, it experienced the second strengthening. On 23 October, it made landfall in the southern Fujian Province and caused the impact of strong wind and heavy rainfall between the coasts of Taiwan Island and mainland China (Qian C. H. et al., 2013 [5]; Chen and Wu, 2016 [7]).

The typhoon track forecast issued by operational meteorological agencies is usually a result of model output calibrated by forecasters. Before the right turn of Megi, three official forecasts issued by the China Meteorological Administration (CMA), Japan Meteorological Agency (JMA), and the Joint Typhoon Warning Center (JTWC) showed that Megi would move northwestward to land in the Hainan Island and western Guangdong Province. Until 1200 UTC on 19 October 2010, the European Centre for Medium-Range Weather Forecast's (ECMWF's) 5-day ensemble mean forecast still predicted the track moving northwestward to the central part of Guangdong. Subsequently after the turning-right point at 1200 UTC on 20 October, the ECMWF 5-day ensemble mean product predicted Megi making landfall in southern Fujian on 23 October. To implement emergency measures, the relevant local governments and meteorological departments have invested a lot of manpower and material resources in Hainan Island and western Guangdong according to the track prediction before 19 October 2010.

What secret does this unusual typhoon hide? What makes it difficult for many models to predict the sudden right turning before even 24 h in advance? According to a Web of Science search, there are 83 papers published for this Megi event and 19 of them focus on track forecasting. Among them, there are many studies that attempt to improve the data assimilation for the initial analysis in different models (Shen and Min 2015 [8]; Kieu et al., 2012 [9]; Li et al., 2013 [10]; Xu et al., 2013 [11]; Chang et al., 2020 [12]). There are papers that studied the effects of environmental fields on the Megi track (Huang et al., 2020 [13]; Wu et al., 2016 [14]). Some papers studied the impacts of improving initialization such as hybrid initialization (combing dynamic and nudging, Wang et al., 2013 [15]) and scale-selective data assimilation (Lai et al., 2014 [16]) on Megi's track. Fewer articles examined the extreme rainfall induced by Megi (Hong et al., 2015 [17]; Chen and Wu, 2016 [7]).

For current or conventional models, the improvement of Megi's track prediction by utilizing the above methods is limited. To understand the mechanism of these unusual TC tracks, a generalized beta advection model (GBAM) was developed (Qian et al., 2014 [18]; Huang et al., 2015 [19]). This is a single-layer global model taken at the pressure layer of minimum anomalous divergence and maximum anomalous vorticity so it can only simulate within 2–4 days. This model has been applied to successfully simulate 15 right-turning TCs in the South China Sea (Qian et al., 2014 [18]) and four left-turning TCs in the East China Sea (Huang et al., 2015 [19]). It is also used in the unusual track prediction of Hurricane Sandy (2012) (Qian et al., 2016 [20]). Sandy is also an unusual super hurricane formed in the North Atlantic with two times of strengthening and left turning (Hall and Sobe, 2013 [21]). The GBAM is developed by using the method of decomposing total wind as the climatological component and anomaly. A dynamic factor in precipitation diagnosis and forecasting is vertical velocity. However, the vertical velocity is still a quantity that is difficult to determine in current numerical models (Gvozdíková and Müller, 2021 [22]). In this paper, we use a novel method of physical decomposition to investigate whether conventional models and traditional synoptic analysis can improve the prediction skill of such unusual TCs. In addition, we introduce another novel theory (called "orthogonal convergence") of anomalous airflow convergence to produce vertical motion for investigating why the ECMWF model is unable to correctly predict the location and intensity of extreme precipitation associated with Typhoon Megi. Both the anomaly-based model and orthogonal convergence have not been well explored in the past. Thus, this paper serves as a promotion of these new ideas. By using tropical cyclone's unusual track and extreme precipitation as samples, the objective is to demonstrate that these new methods can do something that a traditional model or approach might not do well. Figure 1 shows the study area's geographical locations relative to the world. The major climatic systems of a main study area (eastern China and western Pacific) during the northern warm season include a subtropical high over the western

Pacific, a storm track to the north of the subtropical high, and an Asian summer monsoon to the west of the subtropical high. The related weather includes active tropical cyclones over the western Pacific (south side of the subtropical high), a rain band shifted northward to North China (northwest edge of the subtropical high) and hot and humid convective weather in South China (the west of the subtropical high).

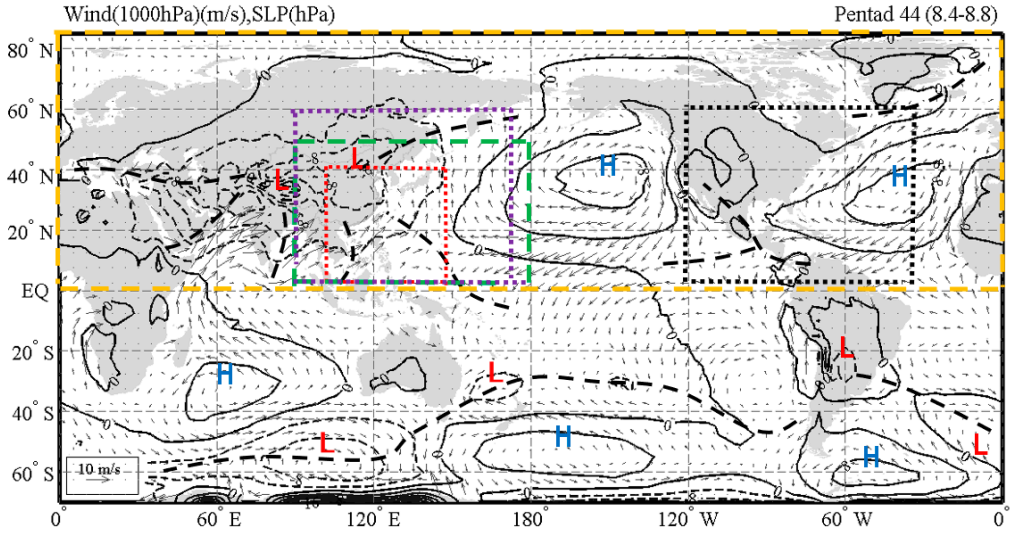

Figure 1. The study area's geographical locations relative to the world. The deviation (solid line, 4 hPa interval) of global sea level pressure relative to 1000 hPa and the surface wind (arrow, m/s) in the pentad 44 (from 4 to 8 August). Letters H and L indicate the centers of high and low pressure. The green dashed-line box is the area (0–60° N, 90–170° E) for Figures 2–4. The red dotted-line box is the area (0–40° N, 100–150° E) for Figure 5. The green dashed-line box is also for Figure 6. The black dotted-line box is the area (0–60° N, 45–120° W) for Figure 7. The yellow dashed-line box is the area of the Northern Hemisphere (0–90° N) for Figure 8. The purple dotted line box is the area (0–50° N, 90–180° E) for Figures 9 and 10.

This paper is organized as follows. After this introduction, datasets, the data decomposition method, orthogonal convergence theory and models are given in Section 2. As an example, the binary interaction of two cyclones is described in Section 3. Anomaly-based variable models and a forecast time-length bottleneck are simulated in Section 4. A comparison of extreme precipitation and conventional model prediction using a dynamical diagnostic parameter is illustrated in Section 5. Finally, discussions and a conclusion are given in Section 6.

2. Datasets/Methods and Theory/Models

2.1. Datasets

Three datasets are used in this paper. The first is the ERA-Interim reanalysis data which can be downloaded from the website (https://www.ecmwf.int/en/forecasts/datasets/reanalysis-datasets/era-interim, accessed on 31 December 2020). The ERA-I is used to calculate the hourly climatological state for the 30-year (1981–2010) period. The second is the model products which can be accessed from "The International Grand Global Ensemble" project (TIGGE, http://apps.ecmwf.int/datasets/data/tigge/levtype=pl/type=cf/, accessed on 30 November 2012). The model ensemble mean forecast products are used to calculate the anomalous variables and parameters. The third is the hourly precipitation based on satellite estimates which can be obtained from the website (https://www.ncei.noaa.gov/products/climate-data-records/precipitation-cmorph, accessed on 30 November 2010) with a horizontal resolution of 0.25 longitude–latitude grid degrees.

2.2. Physical Decomposition of Atmospheric Variables

An atmospheric variable at a spatial point can be physically decomposed as a daily 24 h cycle and annual 365 d cycle (total 8760 h intervals) (Qian et al., 2021 [23]). The hourly climatology can be estimated by averaging observational or reanalysis data on calendar date d over M years,

$$\widetilde{v}_d(\lambda, \varphi, p, t) = \sum_{y=1}^{M} v_{(d,y)}(\lambda, \varphi, p, t)/M. \quad (1)$$

The local hourly or minute-scale temporal climatology does not need to be predicted. An anomalous variable $v'_{(d,y)}(\lambda, \varphi, p, t)$ can be extracted from a total variable $v_{(d,y)}(\lambda, \varphi, p, t)$ by subtracting the temporal climatology $\widetilde{v}_d(\lambda, \varphi, p, t)$,

$$v'_{(d,y)}(\lambda, \varphi, p, t) = v_{(d,y)}(\lambda, \varphi, p, t) - \widetilde{v}_d(\lambda, \varphi, p, t) \quad (2)$$

where λ, φ, p, t are, respectively, longitude, latitude, pressure, and time so that the term (λ, φ, p, t) indicates a point of space and time, y = 1 and M = 30, for 30 years from 1981 to 2010.

2.3. Orthogonal Convergence of Airflows

Three types of horizontal airflow convergence appear in daily weather charts, including wind velocity (tailgating) convergence, wind direction (head-on) convergence, and any angle (cross) convergence between two horizontal airflows. All air masses (or airflows) move on the curved surface of the Earth and are curvilinear motions associated with cyclones or anticyclones. Therefore, the converging horizontal airflow has a centripetal force. Usually, only converging horizontal airflows can produce extreme weather. The shear stress $\vec{\tau}_H$ generated by the cross convergence between two horizontal airflows at point H is

$$\vec{\tau}_H = \left(\frac{m_A}{r_A} v_A^2\right) \cdot \left(\frac{m_B}{r_B} v_B^2\right) \cdot \left(\vec{n}_A \times \vec{n}_B\right) \quad (3)$$

where two horizontal airflow masses (m_A, m_B), which can be seen as two mass points, have their velocities (v_A, v_B) and moving radiuses (r_A, r_B). The directions of shear stress are perpendicular to the plane $\left(\vec{n}_A \times \vec{n}_B\right)$ of two horizontal airflows or two mass points. The shear stress $\vec{\tau}_H$ is a new force in the vertical direction, which is the interactive result of two horizontal airflow centripetal forces. In fact, Equation (3) dynamically presents the collision of two horizontal airflows or two mass points. But, in the weather chart, Equation (3) shows the convergence of two horizontal airflows. The stress modulus for the cross convergence with an angle δ between two horizontal airflows is (Qian et al., 2023 [24])

$$\tau_H = \left(\frac{m_A}{r_A} v_A^2\right) \cdot \left(\frac{m_B}{r_B} v_B^2\right) \cdot sin\delta \quad (4)$$

If the two horizontal airflows are orthogonally collided or converged (δ = 90 degrees) and $r_A = r_B = r$ with the same radius, such as two airflows, are vertically located on the two sides of a shear line, the stress modulus reaches the maximum, i.e., $\tau_{Hmax} = (4/r^2)$ $E_A E_B$. If $E_A = E_B = E = 1/2mv^2$ with the same mass and speed of two airflows on the two sides of a shear line, the energy density for the orthogonal collision or convergence of two airflows at point H is $4E^2$ per unit area r^2. The energy density of two airflows colliding linearly (head-on collision) is $2E$, which is the energy of a combined centroid system of two airflows like two particles with a linear collision (Workman et al., 2022 [25]).

The stress modulus with high energy density is a dynamical indicator of vertical velocity or atmospheric updraft. Usually, horizontal anomalous airflows are stronger in the upper troposphere, so a larger anomalous stress modulus or stronger vertical velocity is located aloft but anomalous moisture is larger in the lower troposphere centered at around

850 hPa. Thus, an indicator or parameter is named as "anomalous moisture stress modulus" (AMSM), which is a collision of two anomalous moisture airflows at 850 hPa,

$$\tau\prime_q = \left(q'_A v'^2_A\right) \cdot \left(q'_B v'^2_B\right) \cdot sin\delta \tag{5}$$

where q'_A and q'_B are the two anomalous moisture masses which are driven by the two horizontal anomalous airflows with their anomalous velocities v'_A and v'_B, and δ is the cross angle between the two anomalous airflows. The AMSM is referred to as a rainfall indicator thereafter.

2.4. Anomaly-Based Variable Single-Level Model

The ECMWF 5-day ensemble mean prediction revealed that Megi should move west–southwestward to enter the central SCS when the model starts to run initially from 15 to 16 October 2010 (Qian C. H., 2013 [5]). Then, Megi should move northwestward in the SCS when the model starts to run initially from 17 to 18 October 2010. Even when starting to run initially from 1200 UTC on 19 October 2010, the model predicted that Megi should move north–northwestward and make landfall at eastern Guangdong Province. However, after 12 h, Megi indeed moved north–northeastward heading to southern Fujian Province. We examined why conventional NWP models cannot predict unusual TC tracks.

We developed the GBAM, a simple single-level global model carrying out two experiments started running, respectively, from 1200 UTC on 16 October and 1200 UTC on 19 October 2010. The GBAM only predicts the anomalous vorticity (Qian et al., 2014 [18]),

$$\frac{\partial \zeta'}{\partial t} = -u\frac{\partial \zeta'}{\partial x} - v\frac{\partial \zeta'}{\partial y} - \beta v'. \tag{6}$$

where u and v are, respectively, total horizontal westerly and southerly winds, the two terms $-u\frac{\partial \zeta'}{\partial x} - v\frac{\partial \zeta'}{\partial y}$ are the advections of total wind to the anomalous vorticity, and the term $-\beta v'$ is the beta advection.

The above model can be decomposed into a linear climatological beta advection model (CBAM),

$$\frac{\partial \zeta'}{\partial t} = -\widetilde{u}\frac{\partial \zeta'}{\partial x} - \widetilde{v}\frac{\partial \zeta'}{\partial y} - \beta v', \tag{7}$$

and a non-linear anomalous beta advection model (ABAM),

$$\frac{\partial \zeta'}{\partial t} = -u'\frac{\partial \zeta'}{\partial x} - v'\frac{\partial \zeta'}{\partial y} - \beta v'. \tag{8}$$

where the two terms $-\widetilde{u}\frac{\partial \zeta'}{\partial x} - \widetilde{v}\frac{\partial \zeta'}{\partial y}$ are the advections of climatological wind to the anomalous vorticity, and the two terms $-u'\frac{\partial \zeta'}{\partial x} - v'\frac{\partial \zeta'}{\partial y}$ are the advections of anomalous wind to the anomalous vorticity.

2.5. Anomaly-Based Variable Multiple-Level Model

Conventional models of operational forecasting are based on total variables governed by a set of primitive equations, such as those used in the ECMWF IFS model. In the China Meteorological Administration (CMA), the operational model is an anomaly-based variable model named the Global/Regional Assimilation and PrEdiction System (GRAPES) (Chen et al., 2008 [26]). A profile of "hydrostatic atmosphere" is introduced as the reference for eliminating the hydrostatical components in the vertical direction of equations. Two large magnitude variables are geopotential height (H) and temperature (T). The former is equivalent to pressure (P) or Exner pressure (Π), while the latter is equivalent to potential temperature (θ). According to Equation (2), two total variables are decomposed as

$$\Pi = \widetilde{\Pi}(\lambda, \varphi, z, t) + \Pi'(\lambda, \varphi, z, t), \tag{9}$$

$$\theta = \widetilde{\theta}(\lambda, \varphi, z, t) + \theta'(\lambda, \varphi, z, t) \tag{10}$$

where z is the height-based-terrain following coordinate which is also like a pressure-based-terrain following coordinate. It is known that $\Pi \approx \widetilde{\Pi} >> \Pi'$ and $\theta \approx \widetilde{\theta} \gg \theta'$, while $\vec{V} \approx \vec{V}'$. The CMA GRAPES is a partial anomaly-based variable model because only two anomalous variables of Π' and θ' are used in the model without considering anomalous wind $\vec{V}'$ and anomalous moisture q'.

It is theoretically possible to develop a global model based on anomaly-based variable equations (Qian and Du, 2022 [27]). We can follow the above three simple anomaly-based variable models (ABAM, CBAM, and GBAM) to get a model of anomaly-based variables based on decomposed climatology and anomaly. Equation (11) shows that it can be decomposed into a linear L part and a nonlinear N part during a step-by-step calculation process,

$$\frac{\partial S'(t)}{\partial t} = -NS'(t) - LS'(t). \tag{11}$$

where S'(t) is a set of anomalous variables such as anomalous wind $\vec{V}\prime$, height (pressure Π'), potential temperature θ' and humidity q'. In the CMA GRAPES model, only two anomalous variables Π' and θ' are introduced. We only give the form of anomalous potential temperature at the local x–y coordinate (Qian and Du, 2022 [27]),

$$\frac{\partial \theta'}{\partial t} = -\left[u'\frac{\partial \theta'}{\partial x} + v'\frac{\partial \theta'}{\partial y} + w'\frac{\partial \theta'}{\partial y}\right] - \left[u'\frac{\partial \widetilde{\theta}}{\partial x} + v'\frac{\partial \widetilde{\theta}}{\partial y} + w'\frac{\partial \widetilde{\theta}}{\partial y}\right] - \left[\widetilde{u}\frac{\partial \theta'}{\partial x} + \widetilde{v}\frac{\partial \theta'}{\partial y} + \widetilde{w}\frac{\partial \theta'}{\partial y}\right] + F_{\theta'}/\widetilde{\Pi} \tag{12}$$

The nonlinear N part (the first part) and linear L parts (the last three parts) on the right-hand side of Equation (12) can be easily separated. In Equation (12), the last part is the external anomalous force relative to the climatological pressure $\widetilde{\Pi}$.

3. Binary Interaction of Two Cyclones

The binary interaction of two atmospheric cyclones is referred to as the Fujiwhara effect, which is a phenomenon that occurs when two cyclones with low-pressure centers move around each other in close distance. This phenomenon is controlled by a large circulation system in the background. The effect is named after S. Fujiwhara, the Japanese meteorologist who initially described this phenomenon (Fujiwhara, 1921 [28]). The binary interaction of a smaller cyclone can influence the development of a larger cyclone or cause two cyclones to merge into one. This effect can be easily observed from two tropical cyclones because total airflows are basically equal to anomalous airflows in the tropics. Many cases in the atmosphere show the interaction between a tropical cyclone and an extratropical cyclone or the interaction between two extratropical cyclones. Typhoon Megi (2010) experienced two-time processes of strengthening and turning. Megi with another tropical cyclone firstly circled counterclockwise from 14 October and finally merged at around 1800 UTC on 17 October 2010, reaching the first peak of intensity. During this period, the track of Megi was driven by the climatological easterly airflow and interacted with an anomalous cyclone. Two anomalous cyclones are controlled by a large circulation system (Qian et al., 2014 [18]).

We focused on the right turning of Megi in the South China Sea. Figure 2 shows the total and anomalous height/temperature cross section along the center of Megi at 0600 UTC on 21 October 2010. This is the stage of Megi reaching the second peak of intensity when it was in the climatological monsoon trough (Lu and Qian, 2012 [29]). In the total height/temperature section, no signal can be used to indicate the super typhoon, except there are several waves in the total temperature (Figure 2a). After the climatological component (Figure 2b) was removed, as seen in Figure 2c, a warm core of Megi is obvious at around 300 hPa. Megi is a deep cyclone, so its negative low-center Lm of anomalous height reached sea level. Other anomalous systems such as a negative low-center L and a positive high-center H of anomalous height are located at the upper troposphere. Usually,

an anomalous high center separates an anomalous warm air mass below and an anomalous cold air mass above and vice versa, which satisfy the hydrostatic equilibrium relationship between height and temperature anomalies (Qian et al., 2016 [30]). These anomalous systems at the upper troposphere should have interacted with each other and driven by the climatological airflows.

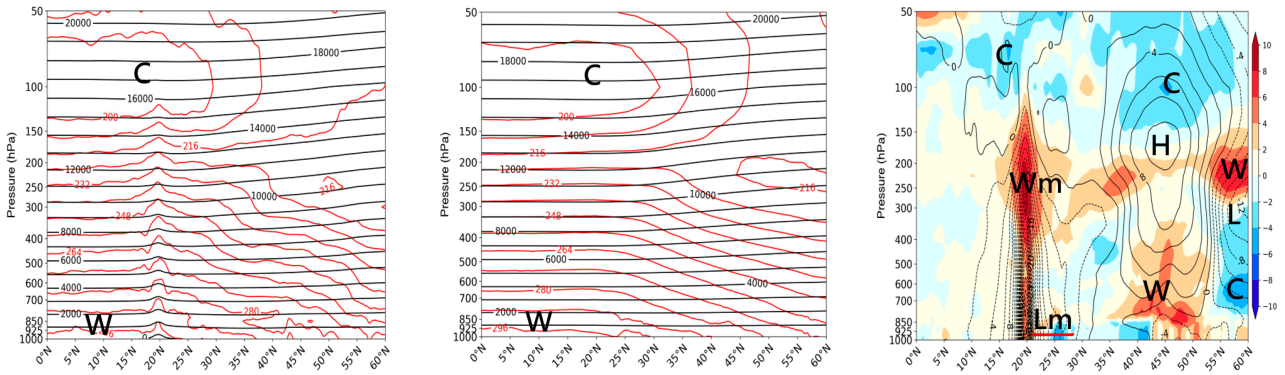

Figure 2. The vertical–latitude section crossing the Megi (2010) center of (**a**) total heights (contour, 200 × 10 gpm interval) and temperature (shading, 10 and 20 K intervals) as well as (**b**) climatological height and temperature using the ERA-Interim product along 117.75° E at 0600 UTC on 21 October 2010. Panel (**c**) is the same as panel (**a**) except for anomalous height (contour, 2 × 10 gpm interval) and temperature (shading, 1 K interval). Letters W/C and H/L indicate warm/cold and high/low centers.

Based on the minimum/maximum anomalous divergence/vorticity and the warm core of Megi after Megi turns right in Figure 2c, Figure 3 gives the total field systems including Megi at 300 hPa. In Figure 3a–c, the subtropical high ridge separates two troughs on the north and three tropical cyclones on the south. The north trough moved eastward to the Sea of Japan and the south trough moved southward to South China at 1200 UTC on 22 October 2010 (Figure 3d). Even on 19 and 20 October 2010, Megi should have moved northwestward according to the traditional synoptic principle because the south trough is too far away from Megi.

Figure 4 shows the anomalous airflow and height at 300 hPa during the four days. On 19 October, the two troughs in Figure 3a become two anomalous cyclones in Figure 4a; the three tropical cyclones including Megi are clearer. The main anomalous systems include an anomalous cyclone in Southwest China, Megi in the South China Sea and an anomalous tropical cyclone in subtropical Northwest Pacific as well as an anomalous anticyclone centered at Japan. We should consider the interaction of these four anomalous systems. However, Megi and the nearby anomalous cyclone "I" are located in a large anomalous system which can clearly indicate that there is a binary interaction or Fujiwhara effect between two anomalous cyclones. Even before the right-turning point such as at 0000 UTC 19 October 2010, two anomalous cyclones were clearly wrapped in a large anomalous system. This is an important mechanism that drives Megi turning northward when the nearby anomalous cyclone "I" moves southeastward. This interaction between two anomalous cyclones can be clearly observed in Figure 4b,c. The anomalous tropical cyclone "III" also entered the large anomalous system (Figure 4c). Finally, Megi and another two anomalous cyclones "I" and "III" merged at 1200 UTC on 22 Octobder 2010 (Figure 4d).

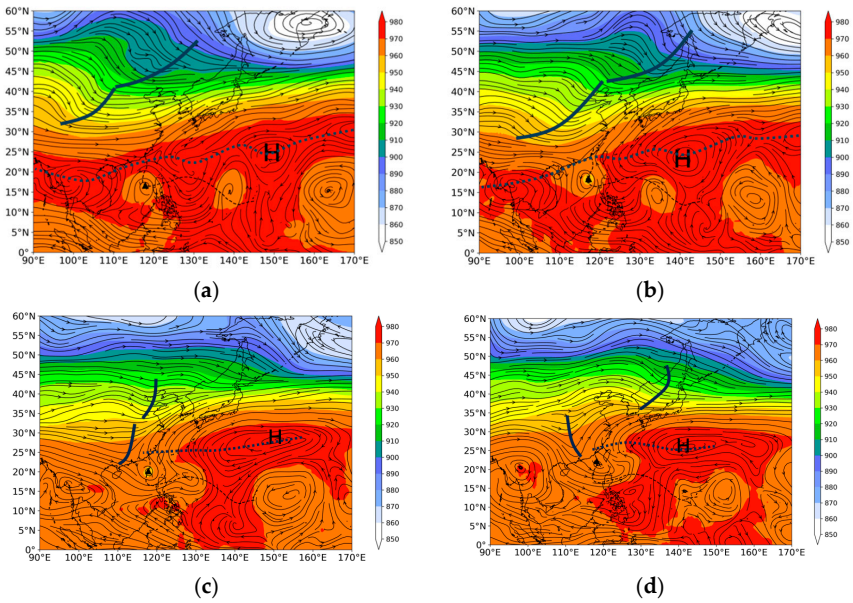

Figure 3. Total airflow and height (shading, 10 × 10 gpm interval) at 300 hPa at 1200 UTC on (**a**) 19, (**b**) 20, (**c**) 21, and (**d**) 22 October 2010. The black sold line is the westerly troughs and the dotted line is the subtropical high ridge line. The black dashed line is the best track of Megi. The triangle sign is the location of Megi and the letter H is the subtropical high. Arrows are airflow lines.

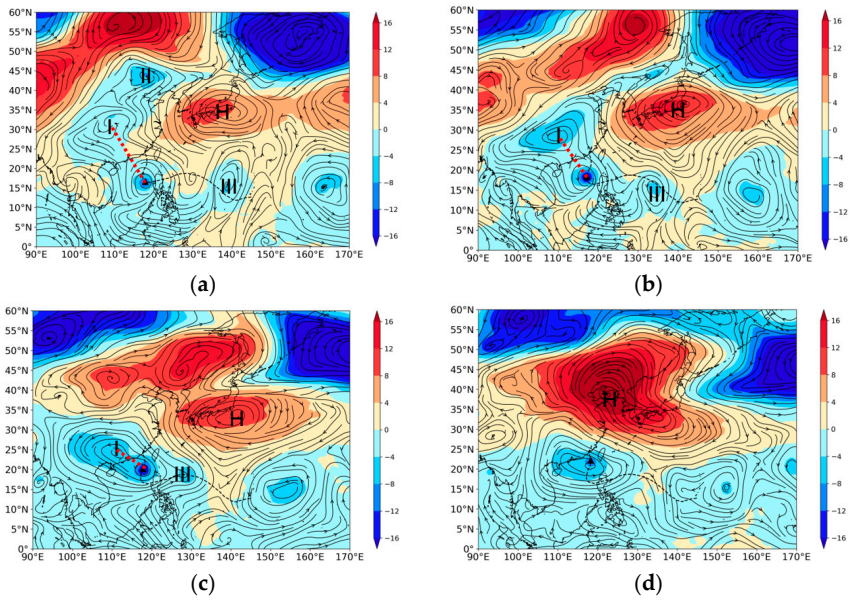

Figure 4. Same as Figure 3 except anomalous airflow and height (shading, 1 × 10, 2 × 10, 3 × 10 and 4 × 10 gpm intervals) at 300 hPa at 1200 UTC on (**a**) 19, (**b**) 20, (**c**) 21, and (**d**) 22 October 2010. Numbers I, II, and III indicate three anomalous cyclones and the letter H is an anomalous anticyclone.

4. Model Results and Forecast Bottleneck

4.1. Single-Level Model Result

As a single-level model, the GBAM is started to experimentally run from 1200 UTC on 16 October 2010. The experimental result shows that the Megi's track is along the green line for the coming 6 days (Figure 5a). It correctly predicts the right turning when Megi arrived to the South China Sea. But the ECMWF ensemble forecast as indicated by the purple dotted line has not predicted the right turning when Megi is in the South China Sea.

The second experiment using three simple models shows the result which started to run from 1200 UTC on 19 October 2010 (Figure 5b). The CBAM predicts a track (circle

purple line) moving west–southwestward, which is forced mainly by the driving of the climatological easterly airflow to the anomalous vorticity of typhoon. The ABAM predicts an anti-clockwise track (square purple line), while the GBAM predicts a track (blue dotted line) that is consistent with the Megi best track (red line). The GBAM's predicted track is also better than the track (purple dotted line) predicted by the ECMWF model during the period of Megi turning right.

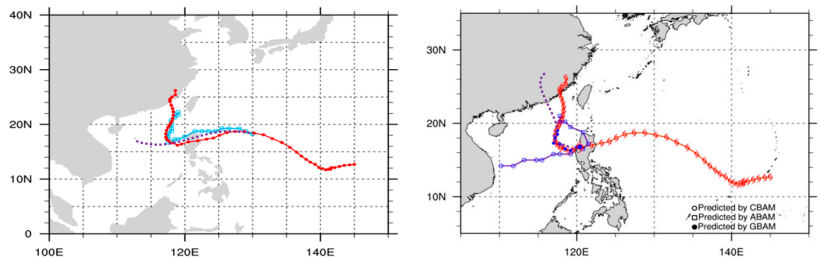

(**a**) (**b**)

Figure 5. (**a**) The ECMWF track forecast (purple dotted line) and the GBAM track forecast (blue circle line) for predicting the Megi best track (red line) initiated to run from 1200 UTC on 16 October 2010. (**b**) The four models of ECMWF (purple dotted line), ABAM (square purple line), CBAM (circle purple line), and GBAM (dot blue line) predict the Megi best track (red line), which are started to run from 1200 UTC on 19 October 2010.

4.2. Multiple-Level Model Result

The anomaly-based variable GRAPES model can simulate the interaction and final merger between Megi and other two anomalous cyclones. The experimental prediction with lead times of 6 days is started to run from 1200 UTC on 16 October 2010. The climatological pressure and temperature during the 6 days from 1200 UTC on 16 October to 1200 UTC on 22 October 2010 is known in the model. The airflows in Figure 6 are calculated by using predicted anomalous pressure based on their geostrophic wind relationship. Figure 6 shows the daily predictions with lead times of 96 h (4 days), 120 h (5 days), and 144 h (6 days). These predictions are consistent with the analysis at 1200 UTC, respectively, on 20 (Figure 4b), 21 (Figure 4c) and 22 (Figure 4d) October 2010. The binary interaction between Megi and another anomalous cyclone "I" in South China at 300 hPa is well simulated. As seen from Figures 4d and 6c, Megi was blocked from moving further northward or northeastward after it made landfall in China because an anomalous anticyclone or anomalous high is centered at Northeast Asia.

In the North Atlantic basin, the infamous Sandy (2012) was an unusual left-turning hurricane and its rapid intensification caused tremendous damage along the Mid-Atlantic and New England regions upon its landfall shortly before 0000 UTC on 30 October 2012 (Galarneau et al., 2013 [31]). The ECMWF model provided an excellent forecast of Sandy's landfall location up to 1 week in advance (Bassill, 2014 [32]). Despite this success, it is of scientific interest to understand the underlying dynamical processes that are responsible for the rapid turning left and intensification of Sandy prior to its landfall.

An experimrntal prediction by using the anomaly-based variable model of CMA GRAPES was also carried out for Sandy's track. Figure 7b–d show the predictions with lead times of 1, 3, and 4 days at 1200 UTC, respectively, on 27, 29, and 30 October 2012. The model started to run from 1200 UTC on 26 October 2012. The spatial distribution of anomalous airflow and height for the four days in Figure 7 are consistent with the analysis result of Qian et al. (2016 [20]). At 1200 UTC on 26 October 2012 (Figure 7a), Sandy should have moved northeastward under the climatological westerly airflow, but it turned left because it interacted with the nearby anomalous low L1. In Figure 7b, Sandy merged with the anomalous low L1, so it reached the first peak of intensity. After that, Sandy should have moved northeastward under the climatological westerly airflow but there were two anomalous lows (L2 and L3) and an anomalous high H1 in the middle latitudes

moving eastward under the climatological westerly airflow. In Figure 7c, Sandy is blocked by an anomalous H1 and interacts with a neighboring low L2. The binary interaction between the hurricane and low L2 caused Sandy to turn left and made it to landfall. The anomalous systems that surround Sandy (2012) are different from ones that surround Megi (2010). At 300 hPa, anomalous lows surrounding Sandy (2012) are all deep, while anomalous lows surrounding Megi are only evident in the upper troposphere.

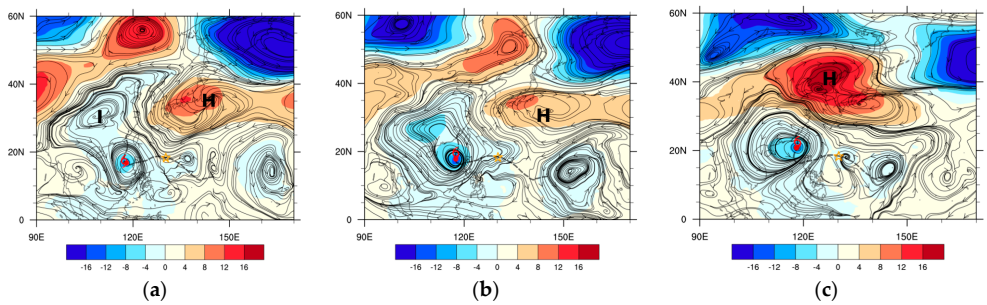

Figure 6. Same as in Figure 4 but is the experimental prediction by using the anomaly-based variable model of CMA GRAPES for the Typhoon Megi (2010) track (blackdashed line). The model is started to run from 1200 UTC on 16 October 2010. Anomalous airflows (vector) and height (shading, 4 × 10 gpm interval) at 300 hPa are predictions at 1200 UTC with lead times of 4, 5, and 6 days, respectively, on (**a**) 20, (**b**) 21, and (**c**) 22 October 2010. The current typhoon position is indicated by a red sign and the yellow star is the initial position of typhoon. The number I indicate an anomalous cyclone and the letter H is an anomalous anticyclone. Arrows are airflow lines.

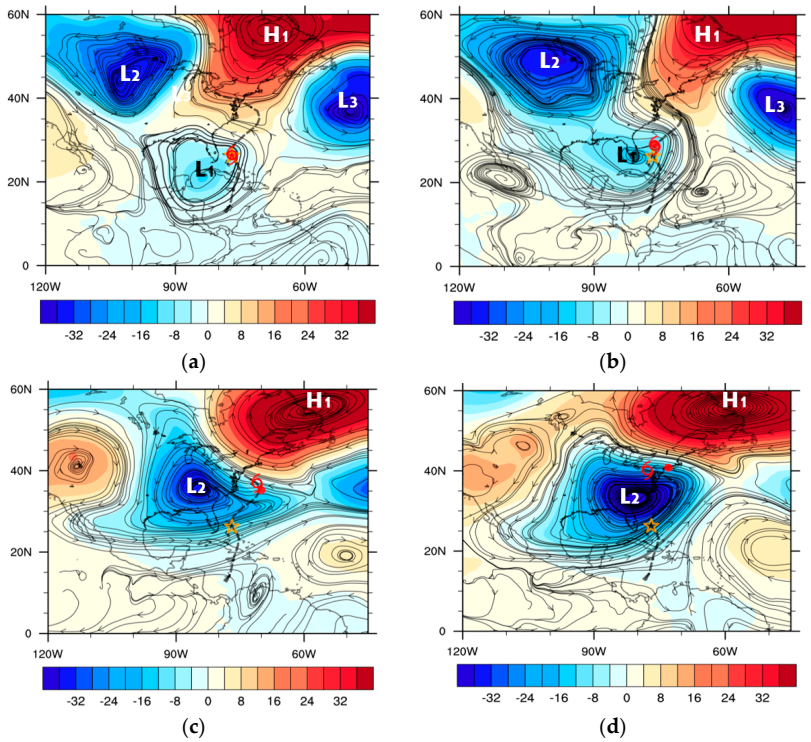

Figure 7. Same as in Figures 4 and 6 but is the experimental prediction by using the anomaly-based variable model of CMA GRAPES for the Hurricane Sandy (2012) track (black dashed line). The model is started to run from 1200 UTC on 26 October 2012. Anomalous airflows and height at 300 hPa are predictions at 1200 UTC with lead times of 0, 1, 3, and 4 days, respectively, on (**a**) 26, (**b**) 27, (**c**) 29 and (**d**) 30 October 2012. Letter H and L are anomalous anticyclones and anomalous cyclones. Arrows are flow lines.

4.3. Bottleneck of Conventional Model

The above two case experiments showed that the ECMWF model can predict the left-turning track of Sandy (2012) for leading 1 week but it cannot predict the right-turning track of Megi (2010) for leading 24 h (1 day). The contrasting results show that there is uncertainty in the TC prediction by the ECMWF model. A statistical result showed that the skill of the ECMWF model in predicting anomalous convergence lines in summer in eastern China is approximately 6.7 days (Qian et al., 2013 [33]). Six dust storms in spring 2021 were originated from Mongolia and moved to Northern China, which are dynamically associated with an anomalous cyclone at 850 hPa (Qian et al., 2022 [34]). The study found that the ECMWF model can predict an anomalous cyclone with an anomalous wind pattern for leading 4–8 days.

Many studies tried to improve the initial field and numerical methods, but it remains difficult to break through the time length bottleneck of leading one-week forecasting for conventional models. It may be a one-week forecasting barrier for all conventional models. We can illustrate this issue with a simple experiment. We only need to use the climatological field at one moment as the initial field that is inputted into the CMA GRAPES model. Theoretically, the output products of the GRAPES model forecast in the coming 10 days should be the climatological field at each time. We use the global climatological field at 0000 UTC on 16 July as the initial field to run the GRAPES model. Figure 8 shows the calculated or predicted climatological height and temperature as well as their anomalies at 0000 UTC on 22 July. The predicted climatological height and temperature at 700 hPa after 6 days should have a smooth spatial distribution. However, there are many synoptic-scale fluctuations. Those centers of height and temperature anomalies relative to their real climatology represent model calculated errors. In Figure 8b, those temperature anomaly centers reach ± 4~5 °C, which can be comparable to the observed temperature anomalies. As indicated in Figure 2c, the maximum height anomaly is located at the upper troposphere (around 300 hPa) and the maximum temperature anomaly is at around 700 hPa. Thus, Figure 8 indicates that all models of primitive equations have a time length bottleneck which is limited by about one week for their predictability, where model forecast errors are comparable to the magnitude of synoptic scale disturbances in the atmosphere.

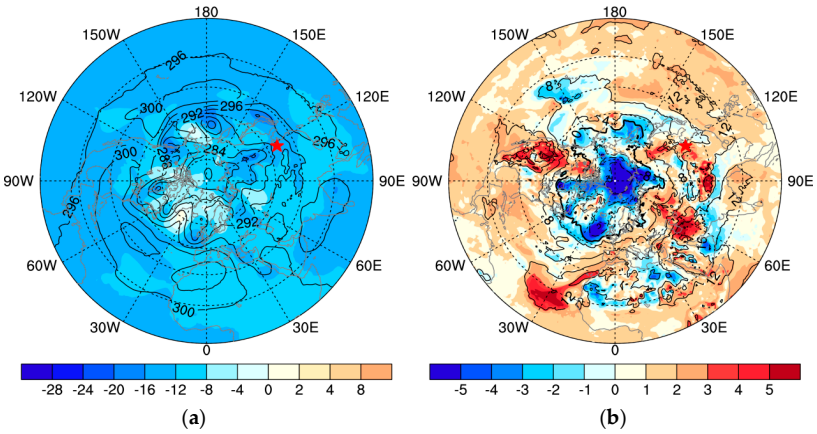

Figure 8. The predicted products of the CMA GRAPES model at 0000 UTC on 22 July with lead times of 6 days. The model is started to run initially by climatological variables from 0000 UTC on 16 July. (**a**) Height (black line, 40 gpm interval) and anomaly (shading, 2 gpm interval) relative to the real climatological height. (**b**) Temperature (black line, 4 K interval) and anomaly (shading, 1 K interval) relative to the real climatological temperature.

5. Extreme Precipitation and Conventional Model Prediction

5.1. Hourly Precipitation and Rainfall Indicator

Extreme precipitation requires the two conditions of strong updraft and saturated water vapor. A tropical cyclone is an extreme weather system that can meet the above

two conditions. Figure 9 gives the hourly precipitation and the AMSM at 850 hPa during Megi when it suddenly turned to the right in the South China Sea but before the final landfall. At 1200 UTC on 19 October 2010 (Figure 9a,b), the hourly precipitation center of Megi is located at the central eastern SCS near the north Philippines, which is consistent with the center of AMSM at 850 hPa. In the Northwest Pacific, some scatter centers of hourly precipitation were not correctly indicated by the AMSM in intensity. We mainly examine the hourly precipitation center more than 4 mm with an AMSM of more than 0.3 as their criteria. From 1200 UTC on 20 October to 1200 UTC on 21 October 2010 (Figure 9c,e), the hourly precipitation center of Megi moved northward and peripheral precipitation reached the coast of mainland China. From the East China Sea to the south and east of Japan, there are patches of precipitation. In Figure 9d,f, the AMSM is a good indication of the spatial distribution of these heavy rainfalls with their criteria (Figure 9c,e).

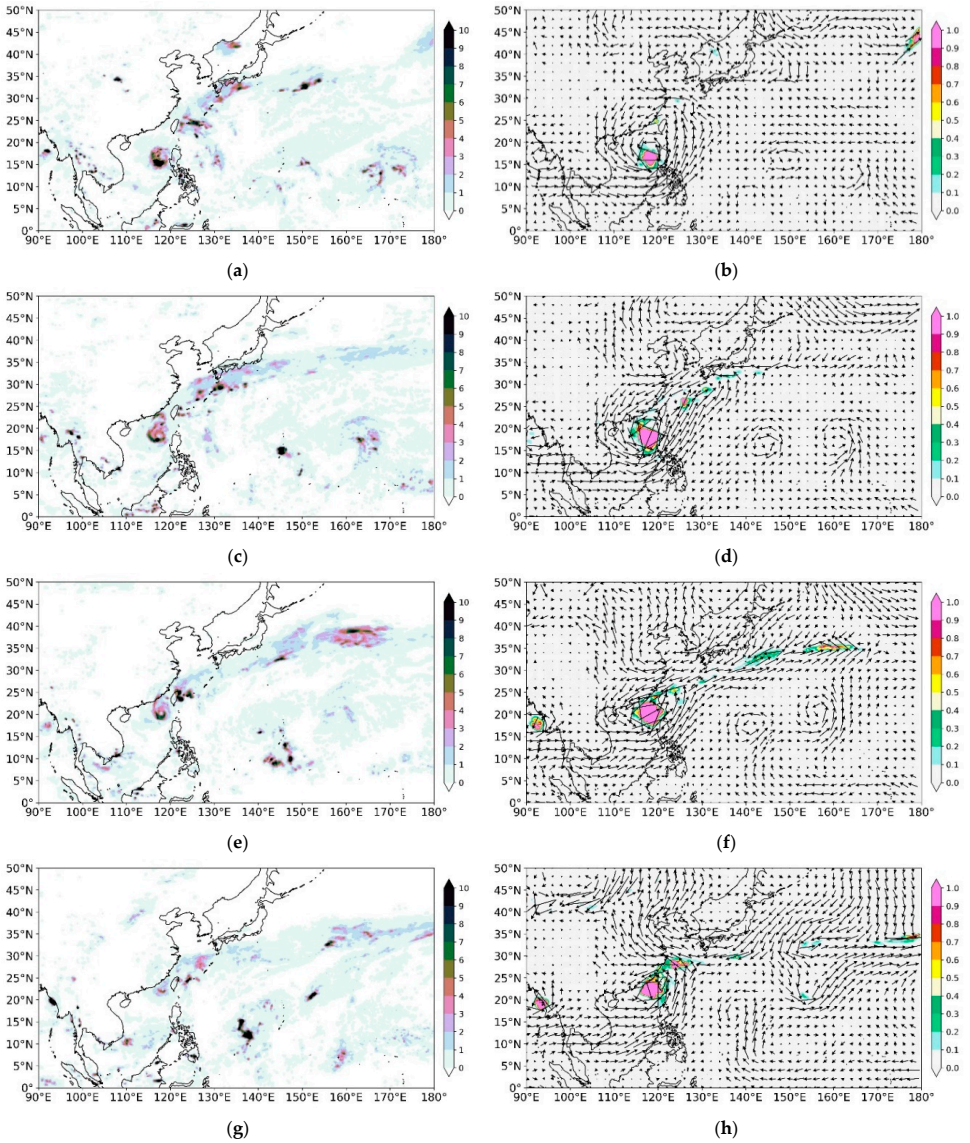

Figure 9. Spatial distribution of (**a**) hourly precipitation (mm/h) based on the satellite estimate at 1200 UTC on 19 October 2010 and (**b**) anomalous moisture stress modulus (AMSM) (shading, 0.03 $m^4 \cdot s^{-4} \cdot kg^2 \cdot kg^{-2}$ interval) with anomalous wind vector (arrow) at 850 hPa at 1200 UTC on 19 October 2010. Panels (**c**,**d**) are the same in panels (**a**,**b**) except at 1200 UTC on 20 October 2010. Panels (**e**,**f**) are at 1200 UTC on 21 October 2010. Panels (**g**,**h**) are at 1200 UTC on 22 October 2010.

The intensity of Megi reached the second strongest on 21 October 2010. From 19 to 22 October 2010, changes in the intensity and position of Megi can also be seen from the AMSM and anomalous systems at 850 hPa (Figure 9b,d,f,h). The hourly precipitation center of Megi can be indicated by AMSM at 850 hPa. Regarding the previous analysis (Qian et al., 2023 [24]), it is difficult to indicate the intensity and location of precipitation by other dynamical parameters such as vorticity and divergence or anomalous vorticity, anomalous divergence, and anomalous kinetic energy of any levels. In Figure 9, the AMSM with a criteria of more than 0.3 at 850 hPa can indicate the corresponding hourly heavy precipitation with a criteria of more than 4 mm following the track of Megi. Here, only one case of Megi for four times is examined. More cases are needed to evaluate the ability of AMSM indicating the hourly precipitation.

5.2. Coventional Model Prediction

The ECMWF model precipitation forecasts are analyzed below for the four days starting from 1200 UTC on 19 October 2010. We, respectively, examine the ECMWF model's forecast of hourly precipitation, Megi location and the diagnosis of AMSM. From 1200 UTC on 19 October to 1200 UTC on 20 October 2010, Megi was experienced a locally turning period for 24 h, so its location change is small. This can be comparable between Figures 9d and 10b where the center of anomalous system and large value center of AMSM are consistent with the analysis while the prediction is with lead times of 24 h. The position of hourly precipitation is observed in Figure 9c while the forecast of rainfall with lead times of 24 h is shown in Figure 10a. For the rainfall prediction, the intensity and area are, respectively, stronger and larger than that of the observed hourly precipitation.

For the observed hourly precipitation of Megi from 20 to 21 October 2010, the intensity has not obviously changed (Figure 9c,e). However, the predicted hourly precipitation from 20 to 21 October 2010 is too heavier in intensity (Figure 10a,c), especially over large areas from the South China Sea to the East China Sea and southern seas of Japan. From 20 to 21 October 2010, the intensity and location of AMSM can be comparable between the prediction (Figure 10b,d) and the analysis (Figure 9c,e). The coverage depends on the AMSA threshold values or criteria used to define "rain".

From 22 to 23 October 2010, the predicted hourly precipitation associated with Megi moved from the offshore to the central and eastern part of Guangdong Province (Figure 10e,g). In Figure 10, the model forecasted hourly heavy rainfall in the southern part of the South China Sea for 4 days. However, precipitation on the southern part of the South China Sea is absent from observations (Figure 9). The AMSM distributions from the analysis (Figure 9) and the prediction (Figure 10) only focus on the center of Megi without the southern part of the South China Sea. The common problem existing in the model is that the area of precipitation forecast is too large, the intensity is too strong, and the position is also greatly shifted. From 1200 UTC on 19 to 1200 UTC on 23 October 2010, the ECMWF model predicted that Megi should move northwestward and approach Hainan Island (Figure 10). The model did not have the ability to predict a right turn that began on 19 October 2010.

The above comparison showed that the error is large for the hourly precipitation predicted by the ECMWF model even for leading 24 h. If the ECMWF model can correctly predict synoptic systems such as the intensity and location of cyclones for leading several days, the AMSM calculated from the model products can well indicate the extreme precipitation. This implies that for the unusual TC track, the accurate precipitation forecast in intensity and location needs anomaly-based variable multiple-level models.

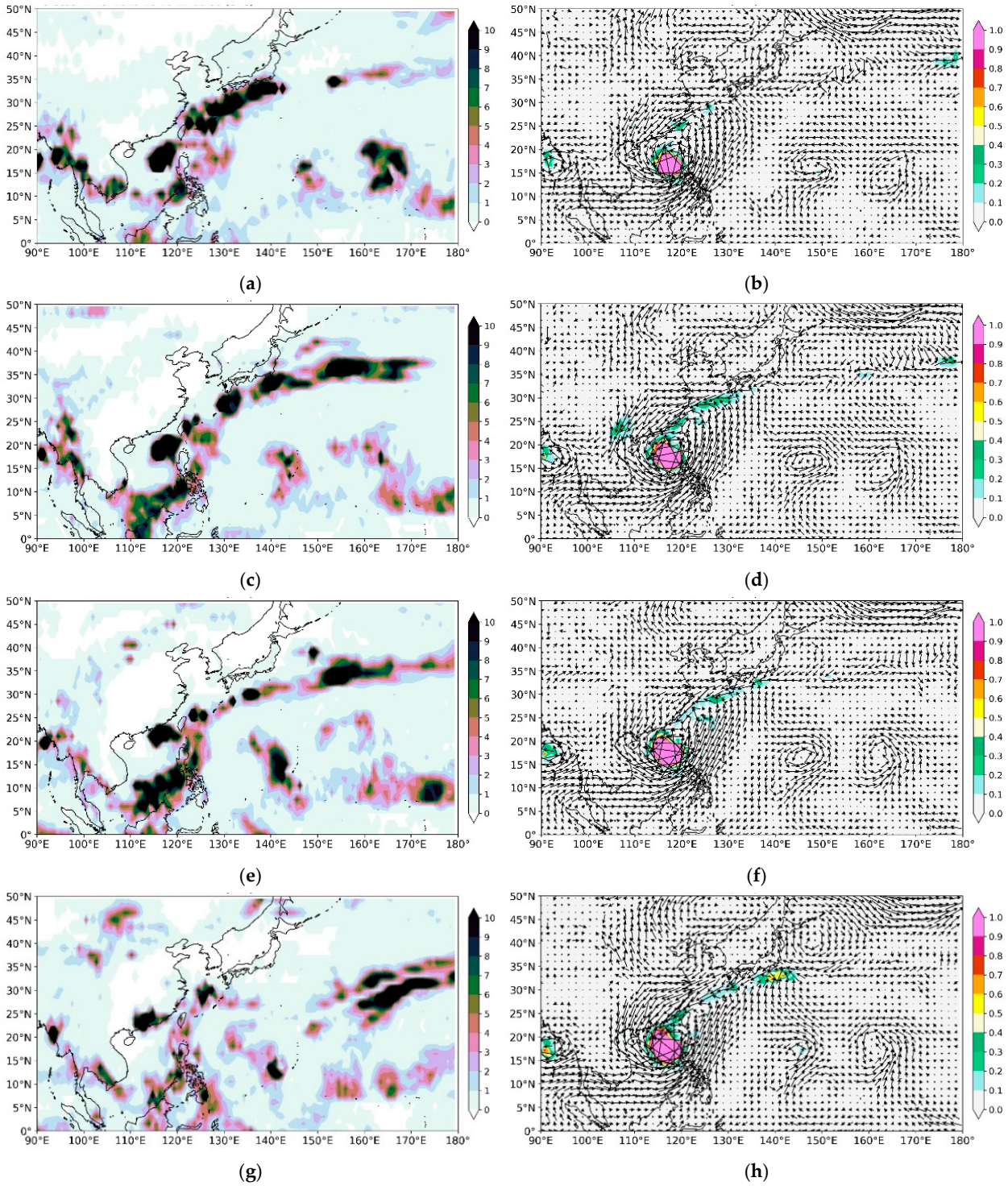

Figure 10. Same in Figure 9a,b except the ECMWF model ensemble mean forecast with lead times of (**a**,**b**) 24, (**c**,**d**) 48, (**e**,**f**) 72, and (**g**,**h**) 96 h at 1200 UTC, respectively, on 20, 21, 22, and 23 October 2010. The model is initially predicted from 1200 UTC on 19 October 2010. The arrow indicates the wind vector.

6. Discussion and Conclusions

6.1. Discussion

Model products have become the main basis of information for extreme weather forecasting in short- and medium-range forecasts (1–2 weeks) (Sillmann et al., 2017 [35]).

The ability to forecast extreme weather should be an important criterion for assessing model performance. The occurrence of extreme weather, such as tropical cyclones with extreme precipitation, is the rapid release of anomalous energy in the atmosphere. Anomalous energy includes anomalous internal energy, anomalous kinetic energy, and anomalous latent heat energy. In Figure 2c, the anomalous warm core over Typhoon Megi (2010) is an example of such anomalous internal energy. In Figure 9, the anomalous cyclone concentrates anomalous kinetic energy and anomalous latent heat energy, as indicated by the AMSM, with anomalous moisture in the lower troposphere. These anomalous energies are linked to three-dimensional atmospheric anomalous systems, such as those in Figure 2c. Therefore, we need to remove the climatological component (Figure 2b) from the total field variables in Figure 2a to obtain the spatial distribution of anomalous variables in Figure 2c. The spatial configuration of these anomalous systems, as well as their intensity and location, need to be predicted in NWP models of operational meteorological agencies.

The idea of operational forecasters needs to be adjusted from the judgment of total variable systems based on the traditional weather chart to the judgment of anomalous variable systems based on the anomalous weather chart. In Figure 3, it is difficult for forecasters to judge the interactions between different systems from the total airflow and height; thus, it is difficult to predict the sudden turn of Megi (2010). However, using anomalous weather charts such as Figure 4, forecasters can judge their interaction and predict Megi's right turn several days in advance.

Forecasters often use the total wind at the 500 hPa layer as steering airflows for TC track forecasting. Figure 5 shows that the TC track is mainly determined by the drive of the climatological airflow in the strongest central layer of TCs and the interaction of adjacent anomalous systems. The climatological variable distribution in the global atmosphere is a dynamic–thermodynamic equilibrium state forced by the solar radiation and influenced by the underlying surface environment. A climatological state can be calculated by averaging observations over many years and do not require forecasting. However, conventional models of primitive equations predict both the climatological component and anomalous variables, resulting in false anomalies, as shown in Figure 8. The growth time of false anomalies associated with the calculation of the climatological component is about 6–7 days, which is a time length bottleneck for the conventional models to forecast extreme weather systems.

An anomaly-based variable model, like the CMA GRAPES model, separates the climatological height (pressure) and temperature components from the anomalous variables. The anomaly-based variable model was able to predict the right turn of the unusual Megi track five days in advance (Figure 6), while the current ECMWF model of primitive equations was not even able to predict the right turn one day in advance (Figure 10). This success story offers hope for the conventional NWP models to overcome this bottleneck.

For accurately predicting the intensity and location of precipitation, in addition to the need for accurately predicting anomalous systems, the calculation of atmospheric vertical velocity is a long-standing unsolved problem. The difference in intensity, timing, and position of precipitation forecasts in conventional NWP models relative to the observation is directly related to the difficulty of accurately determining vertical velocity. In addition to the anomalous water vapor, the proposed dynamic moisture parameter AMSM as a rainfall indicator contains the factor of vertical velocity. The factor of vertical velocity is the shear stress modulus formed by the orthogonal collision of horizontal anomalous airflows. It is a process transformed from the collision energy of horizontal anomalous airflows to the energy of vertical motion. Although the conventional NWP model contains everything such as divergence and vorticity of the horizontal airflows, the dynamic process of orthogonal convergence caused by horizontal anomalous airflows needs to be emphasized or highlighted in the future NWP models.

6.2. Conclusions

This paper summarized and proposed a novel method and a novel theory. This novel method is to physically decompose the total atmospheric variables of observed or model products into climatology and an anomalous component. Using the anomalous components, forecasters can infer future trends of anomalous systems, such as the future movement of the TC which will be steered by climatological airflows and the interactions between anomalous systems (Qian et al., 2014 [18]; Huang et al., 2015 [19]). Using the spatial structure or patterns of the geopotential height/temperature anomalies and the wind/humidity anomalies, forecasters can determine the type, intensity, location, and timing of extreme weather events (Qian et al., 2021 [23]). If the conventional model forecasts are accurate, the extreme weather can be localized, intensified, and timed by the anomalous components (Qian, 2017 [36]). In the past decade, this physical decomposition method has been applied to the diagnosis and prediction of extreme weather events such as heavy rainfall (Shan et al., 2015 [37]; Qian et al., 2021 [38]), heat waves (Chen et al., 2016 [39]), low temperatures or cold events (Shi et al., 2021 [40]; Qian et al. 2016 [41]), haze (Qian and Huang, 2019 [42]), ozone (Qian et al., 2022 [43]), tornadoes (Qian et al., 2017 [44]), sandstorms (Qian et al., 2022 [34]), wide fires (Qian et al., 2021 [45]), etc. In the future, machine learning of anomalous systems would improve the ability to predict extreme weather.

This novel theory described that the orthogonal collision of horizontal anomalous airflows can form a vertical motion and anomalous energies. For a long time, determining the location and intensity of the vertical movement that leads to extreme precipitation has been a difficult problem. This theory dynamically links the convergence of horizontal anomalous airflows and forms a vertical motion. Extreme precipitation requires a combination of water vapor and vertical movement conditions in the lower troposphere. In this paper, the AMSM at the 850 hPa layer is a good combination of water vapor and vertical motion conditions. In future, this parameter can be introduced into the extreme precipitation forecast based on the interpretation application of model products, or it can be directly introduced into NWP models to improve the accuracy of precipitation forecasting.

At present, conventional medium-range NWP models are faced with the problem of a one-week forecasting barrier. This paper reveals that the forecasting barrier may be due to an increase in the calculation error of climatological variables in the conventional NWP models of primitive equations. In future, anomaly-based variable models can be developed experimentally, and climatology as a known force can extend the forecast timeliness.

Orthogonal collision theory can be applied not only to explain theoretical and practical problems in extreme weather phenomena, but also to other disciplines. In terms of explaining tornado formation, orthogonal collisions of horizontal airflow in the lower atmosphere can form not only rotating cumulonimbus clouds, but also rotating funnel-shaped clouds—tornadoes (Qian et al., 2023 [24]). This theory can explain the dynamics of super typhoons, such as the orthogonal collision of horizontal airflow in the upper atmosphere, which can form a downdraft (eye) in the center of the super TC and a cloud–rain ring corresponding to the surrounding updraft (Qian, 2023 [46]). This theory can explain astronomical optical phenomena such as gravitational lensing and auroras (Qian, 2023 [47], 2023 [48]). It can explain the traces left by the Big Bang, such as the motion relationship between stars, including the precession of Mercury (Qian, 2023 [49]; Qian, 2024 [50]). It can be applied in high-energy physics, such as the construction of orthogonal collision colliders (Qian, 2022 [51]). It can explain the continental drift and orogeny in the early Earth period (Qian et al., 2023 [52]).

To help readers understand the whole picture of this anomaly-based research topic that we are exploring, Figure 11 outlines the main themes with represented references. There are four major aspects including (a) anomaly-based weather charts (Qian et al., 2021 [23]); (b) anomaly-based diagnostic parameters or index (Qian et al., 2017 [44], Qian et al., 2015 [53]); (c) anomaly-based prediction model (Qian et al., 2014 [18], Huang et al., 2015 [19], and Qian and Du 2022 [27]); and (d) anomaly-based post-processing of model forecasts

(Du and Deng 2022 [54]). There are still two blank areas needing to be explored in future: the anomaly-based variable full NWP model and anomaly-based variable AI model (circled by dash lines and highlighted in red in Figure 11).

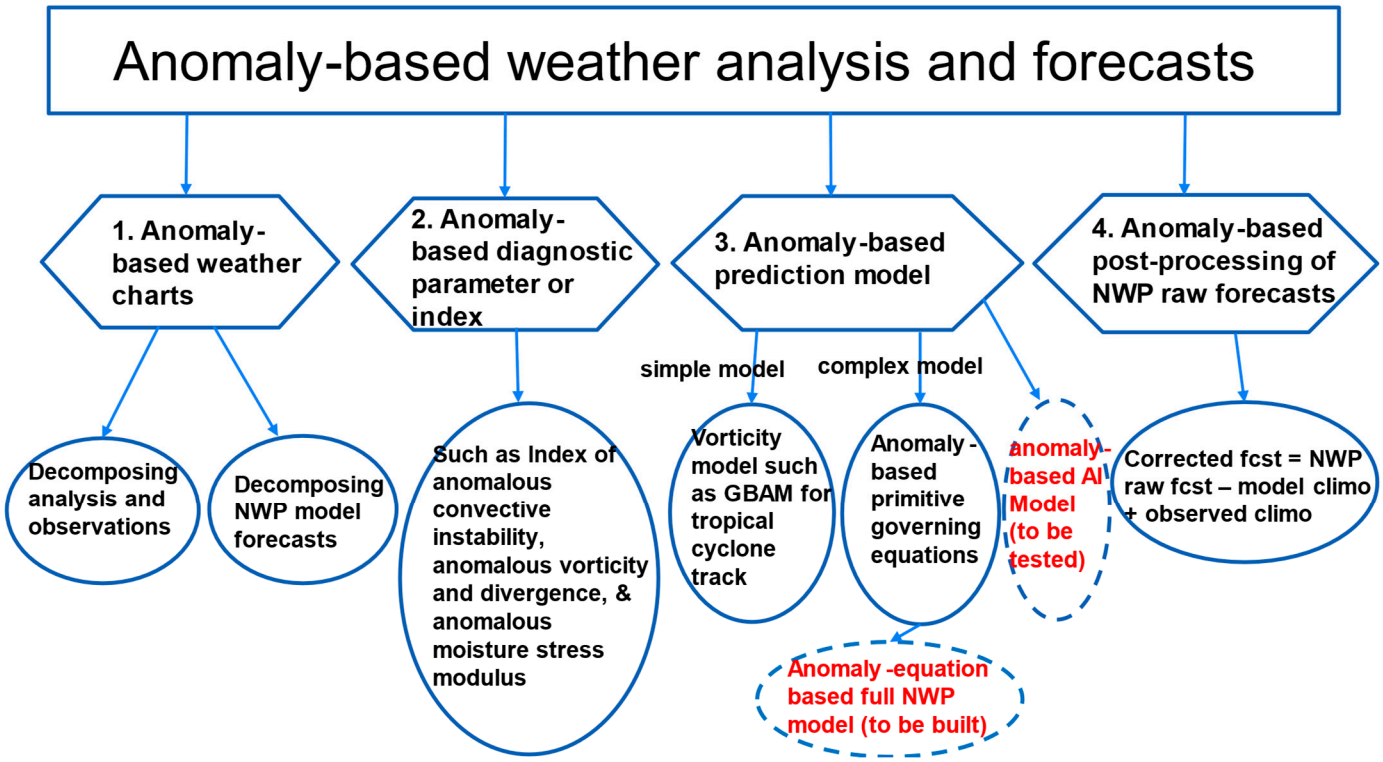

Figure 11. An outline of the anomaly-based variable weather analysis and forecast research areas. There are four aspects: (1) anomaly-based weather charts (Qian et al., 2021 [23]); (b) anomaly-based diagnostic parameters or index (Qian et al., 2017 [44], Qian et al., 2015 [53], and the AMSM in this article); (c) anomaly-based prediction model (Qian et al., 2014 [18], Huang et al., 2015 [19], and Qian and Du 2022 [27]); and (d) anomaly-based post-processing of model forecasts (Du and Deng 2022 [54]). The solid circled areas are those that have been investigated by the authors, while the dashed circled areas (marked in red) are those that need to be investigated in future.

Author Contributions: W.Q.: Conceptualization, methodology, writing—original draft, writing—review and editing; J.D.: formal analysis, writing—review and editing; Y.A. and J.L.: drawing and calculating; Y.L.: running model; and J.X.: formal analysis, funding acquisition. All authors have read and agreed to the published version of the manuscript.

Funding: This study was jointly supported by the National Natural Science Foundation of China (72293604, 42130605, and 41775067) and Shenzhen Nature Science Foundation (JCYJ20210324131810029).

Data Availability Statement: The ERA-Interim reanalysis data are from the website (https://www.ecmwf.int/en/forecasts/datasets/reanalysis-datasets/era-interim, accessed on 31 December 2020). The model products are from the TIGGE (http://apps.ecmwf.int/datasets/data/tigge/levtype=pl/type=cf/, accessed on 30 November 2012). The hourly precipitation is from the website (https://www.ncei.noaa.gov/products/climate-data-records/precipitation-cmorph, accessed on 30 November 2010).

Acknowledgments: Authors wish to thank three anonymous reviewers for their constructive suggestions and comments which have improved the paper.

Conflicts of Interest: The authors declare no conflicts of interest.

References

1. Maxwell, J.T.; Bregy, J.C.; Robeson, S.M.; Knapp, P.A.; Soule, P.T.; Trouet, V. Recent increases in tropical cyclone precipitation extremes over the US east coast. *Proc. Natl. Acad. Sci. USA* **2021**, *118*, e2105636118. [CrossRef] [PubMed]
2. Li, Y.; Zhao, D.J. Climatology of tropical cyclone extreme rainfall over China from 1960 to 2019. *Adv. Atmos. Sci.* **2022**, *39*, 320–332. [CrossRef]
3. Marchok, T. Important factors in the tracking of tropical cyclones in operational models. *J. Appl. Meteorol. Climatol.* **2021**, *60*, 1265–1284. [CrossRef]
4. Conroy, A.; Titley, H.; Rivett, R.; Feng, X.; Methven, J.; Hodges, K.; Brammer, A.; Burton, A.; Chakraborty, P.; Chen, G.; et al. Track forecast: Operational capability and new techniques—Summary from the Tenth International Workshop on Tropical Cyclones (IWTC-10). *Trop. Cyclone Res. Rev.* **2023**, *12*, 64–80. [CrossRef]
5. Qian, C.H.; Zhang, F.Q.; Green, B.; Zhang, J.; Zhou, X.Q. Probabilistic Evaluation of the Dynamics and Prediction of Supertyphoon Megi (2010). *Weather Forecast.* **2013**, *28*, 1562–1577. [CrossRef]
6. Yu, H.; Chen, G.; Zhou, C.; Wong, W.K.; Yang, M.; Xu, Y.; Chen, P.; Wan, R.; Hu, X. Are we reaching the limit of tropical cyclone track predictability in the western North Pacific? *Bull. Amer. Meteorol. Soc.* **2021**, *103*, E410–E428. [CrossRef]
7. Chen, T.C.; Wu, C.C. The remote effect of Typhoon Megi (2010) on the heavy rainfall over northeastern Taiwan. *Mon. Weather Rev.* **2016**, *144*, 3109–3131. [CrossRef]
8. Shen, F.F.; Min, J.Z. Assimilating AMSU-A radiance data with the WRF hybrid En3DVAR system for track predictions of Typhoon Megi (2010). *Adv. Atmos. Sci.* **2015**, *32*, 1231–1243. [CrossRef]
9. Kieu, C.Q.; Truong, N.M.; Mai, H.T.; Ngo-Duc, T. Sensitivity of the track and intensity forecasts of Typhoon Megi (2010) to satellite-derived atmospheric motion vectors with the ensemble Kalman filter. *J. Atmos. Ocean Technol.* **2012**, *29*, 1794–1810. [CrossRef]
10. Li, X.F.; Zhao, K.; Wang, M.; Ming, J. Short-term forecasting of super typhoon Megi at landfall through cycling assimilation of China coastal radar data. *J. Meteorol. Sci.* **2013**, *33*, 3.
11. Xu, D.; Liu, Z.; Huang, X.-Y.; Min, J.; Wang, H. Impact of assimilating IASI radiance observations on forecasts of two tropical cyclones. *Meteorol. Atmos. Phys.* **2013**, *122*, 1–18. [CrossRef]
12. Chang, Y.-P.; Yang, S.-C.; Lin, K.-J.; Lien, G.-Y.; Wu, C.-M. Impact of tropical cyclone Initialization on its convection development and intensity: A case study of Typhoon Megi (2010). *J. Atmos. Sci.* **2020**, *77*, 443–464. [CrossRef]
13. Huang, Q.J.; Ge, X.Y.; Peng, M. Impacts of an upper-level easterly wave on the sudden track change of Typhoon Megi (2010). *J. Meteorol. Soc. Jpn.* **2020**, *98*, 1335–1352. [CrossRef]
14. Wu, C.C.; Tu, W.; Pun, I.; Lin, I.; Peng, M.S. Tropical cyclone-ocean interaction in Typhoon Megi (2010)—A synergy study based on ITOP observations and atmosphere-ocean coupled model simulations. *J. Geophys. Res.-Atmos.* **2016**, *121*, 153–167. [CrossRef]
15. Wang, H.; Wang, Y.Q.; Xu, H.M. Improving simulation of a tropical cyclone using dynamical initialization and large-scale spectral nudging: A case study of Typhoon Megi (2010). *Acta Meteorol. Sin.* **2013**, *27*, 455–475. [CrossRef]
16. Lai, Z.J.; Hao, S.; Peng, S.; Liu, B.; Gu, X.; Qian, Y.-K. On improving tropical cyclone track forecasts using a scale-selective data assimilation approach: A case study. *Nat. Hazards* **2014**, *73*, 1353–1368. [CrossRef]
17. Hong, J.-S.; Fong, C.-T.; Hsiao, L.-F.; Yu, Y.-C.; Tzeng, C.-Y. Ensemble Typhoon Quantitative Precipitation Forecasts Model in Taiwan. *Weather Forecast.* **2015**, *30*, 217–237. [CrossRef]
18. Qian, W.; Shan, X.; Liang, H.; Huang, J.; Leung, C.H. A generalized beta advection model to improve unusual typhoon track prediction by decomposing total flow into climatic and anomalous flows. *J. Geophys. Res. Atmos.* **2014**, *119*, 1097–1117. [CrossRef]
19. Huang, J.; Du, J.; Qian, W. A comparison between generalized beta-advection model and classical beta-advection model in predicting and understanding unusual typhoon tracks in eastern China seas. *Weather Forecast.* **2015**, *30*, 771–792. [CrossRef]
20. Qian, W.; Huang, J.; Du, J. Examination of Hurricane Sandy's (2012) structure and intensity evolution from full-field and anomaly-field analyses. *Tellus A Dyn. Meteorol. Oceanogr.* **2016**, *68*, 29029. [CrossRef]
21. Hall, T.M.; Sobe, A.H. On the impact angle of Hurricane Sandy's New Jersy landfall. *Geophys. Res. Lett.* **2013**, *40*, 2312–2315. [CrossRef]
22. Gvozdíková, B.; Müller, M. Predictability of moisture flux anomalies indicating central European extreme precipitation events. *Q. J. R. Meteorol. Soc.* **2021**, *147*, 3335–3348. [CrossRef]
23. Qian, W.; Du, J.; Ai, Y. A review: Anomaly-based versus full-field-based weather analysis and forecasting. *Bull. Am. Meteorol. Soc.* **2021**, *102*, E849–E870. [CrossRef]
24. Qian, W.; Du, J.; Leung, J.C.; Li, W.; Wu, F.; Zhang, B. Why are severe weather and anomalous climate events mostly associated with the orthogonal convergence of airflows? *Weather Clim. Extrem.* **2023**, *42*, 100633. [CrossRef]
25. Particl Data Group; Workman, R.L.; Burkert, V.D.; Crede, V.; Klempt, E.; Thoma, U.; Tiator, L.; Agashe, A.; Aielli, G.; Allanach, B.C.; et al. Review of Particle Physics. *Prog. Theor. Exp. Phys.* **2022**, *2022*, 083C01.
26. Chen, D.H.; Xue, J.; Yang, X.; Zhang, H.; Shen, X.; Hu, J.; Wang, Y.; Ji, L.; Chen, J. New generation of multi-scale NWP system (GRAPES): General scientific design. *Chin. Sci. Bull.* **2008**, *53*, 3433–3445. [CrossRef]
27. Qian, W.; Du, J. Anomaly format of atmospheric governing equations with climate as a reference atmosphere. *Meteorology* **2022**, *1*, 127–141. [CrossRef]
28. Fujiwhara, S. The natural tendency towards symmetry of motion and its application as a principle in meteorology. *Q. J. R. Meteorol. Soc.* **1921**, *47*, 287–293. [CrossRef]

29. Lu, B.; Qian, W. Seasonal lock of rapidly intensifying typhoons over the South China offshore in early fall. *Chin. J. Geophys.* **2012**, *55*, 1523–1531.
30. Qian, W.; Huang, J.; Zhang, G.W. Reexamining the binary interaction of four pairs of tropical cyclones in the Northwest Pacific. *J. Meteorol. Soc. Jpn.* **2016**, *94*, 303–322. [CrossRef]
31. Galarneau, T.J.; Davis, C.A.; Shapiro, M.A. Intensification of Hurricane Sandy (2012) through extratropical warm core seclusion. *Mon. Weather Rev.* **2013**, *141*, 4296–4321. [CrossRef]
32. Bassill, N.P. Accuracy of early GFS and ECMWF Sandy (2012) track forecasts: Evidence for a dependence on cululus parameterization. *Geophys. Res. Lett.* **2014**, *41*, 3274–3281. [CrossRef]
33. Qian, W.; Li, J.; Shan, X. Application of synoptic-scale anomalous winds predicted by medium-range weather forecast models on the regional heavy rainfall in China in 2010. *Sci. China (Earth Sci.)* **2013**, *56*, 1059–1070. [CrossRef]
34. Qian, W.; Leung, J.; Ren, J.; Du, J.; Feng, Y.; Zhang, B. Anomaly based synoptic analysis and model prediction of six dust storms moving from Mongolia to northern China in Spring 2021. *J. Geophys. Res.-Atmos.* **2022**, *127*, e2021JD036272. [CrossRef]
35. Sillmann, J.; Thorarinsdottir, T.; Keenlyside, N.; Schaller, N.; Alexander, L.V.; Hegerl, G.; Seneviratne, S.I.; Vautard, R.; Zhang, X.; Zwiers, F.W. Understanding, modeling and predicting weather and climate extremes: Challenges and opportunities. *Weather Clim. Extrem.* **2017**, *18*, 65–74. [CrossRef]
36. Qian, W. *Temporal Climatology and Anomalous Weather Analysis*; Springer Atmospheric Sciences; Springer: Singapore, 2017; 687p, ISSN 2194-5225. [CrossRef]
37. Shan, X.L.; Jiang, N.; Qian, W. Regional heavy rain locations associated with anomalous convergence lines in eastern China. *Nat. Hazards* **2015**, *77*, 1731–1750. [CrossRef]
38. Qian, W.; Ai, Y.; Leung, J.; Zhang, B.L. Anomaly-based synoptic analysis and model product application for 2020 summer southern China rainfall events. *Atmos. Res.* **2021**, *258*, 105631. [CrossRef]
39. Chen, Y.; Hu, Q.; Yang, Y.M.; Qian, W. Anomaly-based analysis of extreme heat waves in Eastern China during 1981–2013. *Inter. J. Climatol.* **2016**, *37*, 509–523. [CrossRef]
40. Shi, J.; Wu, K.J.; Qian, W.; Huang, F.; Li, C.; Tang, C. Characteristics, trend, and precursors of extreme cold events in northwestern North America. *Atmos. Res.* **2021**, *249*, 105338. [CrossRef]
41. Qian, W.; Yu, T.; Du, J. A unified approach to trace surface heat and cold events by using height anomaly. *Clim. Dyn.* **2016**, *46*, 1647–1664. [CrossRef]
42. Qian, W.; Huang, J. Applying the anomaly-based weather analysis on Beijing severe haze episodes. *Sci. Total Environ.* **2019**, *647*, 878–887. [CrossRef] [PubMed]
43. Qian, W.; Xu, M.; Ai, Y. Anomaly-based synoptic analysis to identify and predict meteorological conditions of strong ozone events in North China. *Air Qual. Atmos. Health* **2022**, *15*, 1699–1711. [CrossRef]
44. Qian, W.; Leung, J.; Luo, W.; Du, J.; Gao, J.D. An index of anomalous convective instability to detect tornadic and hail storms. *Meteorol. Atmos. Phys.* **2017**, *131*, 351–373. [CrossRef]
45. Qian, W.; Ai, Y.; Yu, J.Y.; Du, J. Opposite anomalous synoptic patterns for potential California large wildfire spread and extinguishing in 2018 cases. *Atmos. Res.* **2021**, *262*, 105804. [CrossRef]
46. Qian, W. Identifying the spatial structure of black hole and tropical cyclone based on a theoretical analysis of orthogonal interaction. *J. Mod. Phys.* **2023**, *14*, 933–952. [CrossRef]
47. Qian, W. A physical explanation for the formation of auroras. *J. Mod. Phys.* **2023**, *14*, 271–286. [CrossRef]
48. Qian, W. On the physical nature of einstein's gravitational lensing effect. *J. High Energy Phys. Gravit. Cosmol.* **2023**, *9*, 383–399. [CrossRef]
49. Qian, W. On the attribution of Mercury's perihelion precession. *J. Appl. Math. Phys.* **2023**, *11*, 1359–1373. [CrossRef]
50. Qian, W. The essence of gravity is the expansion tendency of the universe after the Big Bang. *J. Mod. Phys.* **2024**, *15*, 804–849. [CrossRef]
51. Qian, W. Orthogonal collision of particles produces new physical state. *J. Mod. Phys.* **2022**, *13*, 1440–1451. [CrossRef]
52. Qian, W.; Leung, J.; Zhang, B. An orthogonal collision dynamic mechanism of wave-like uplift plateaus in southern Asia. *Open J. Geol.* **2023**, *13*, 828–846. [CrossRef]
53. Qian, W.; Du, J.; Shan, X.; Jiang, N. Incorporating the effects of moisture into a dynamical parameter: Moist vorticity and moist divergence. *Weather Forecast.* **2015**, *30*, 1411–1428. [CrossRef]
54. Du, J.; Deng, G. How should a numerical weather prediction be used: Full field or anomaly? A conceptual demonstration with a Lorenz model. *Atmosphere* **2022**, *13*, 1487. [CrossRef]